Article

Multilayer stretchable electronics with designs enabling a compact lateral form

Check for updates

Dongwuk Jung [1], Hunpyo Ju[1,2], Sungbum Cho[1], Taeyeon Lee[1], Changeui Hong[1] & Jongho Lee [1] ✉

Stretchable electronics are of huge interest as they can be useful in various irregular non-planar or deformable surfaces including human bodies. High density multi-functional stretchable electronics are beneficial as they can be reliably used in more compact regions. However, simply stacking multiple layers may increase induced strain, reducing degree of stretchability. Here, we present the design approach for the stretchable multilayer electronics that provide a similar degree of stretchability compare to a single layer electronics although the multilayer electronics are in much more compact form. We provide experimental and computational analyses for the benefits of the approach along with demonstrations with compact form of the multi-functional stretchable implantable bio-electronics and of the stretchable multilayer passive matrix LEDs array. The results presented here should be useful for a wide range of applications that require stretchable high-density electronics.

Stretchable electronics capable of deforming to external forces broaden application of electronics very widely including curved surfaces[1–3], skin-like surfaces[4–8], and even subcutaneous regions[9–13]. Recently, stretchable electronics are being developed to provide multiple functions with more complex designs such as multiple bio-signal sensing[5,7], feedback signaling[6,13,14], optoelectronic systems[15,16], multifunctional soft robots[17,18], and communication with other devices[4,8,9,19] which naturally require a higher number of electronic components and more complex routing traces, resulting in relatively larger electronics size. However, whenever possible, smaller electronics for the same functions provide convenience in many applications like bio-signal sensing in specific sites[2,9,20], minimum invasive surgeries[21,22], or minimized high-density electronics[23,24].

One of the most promising methods is laminating or stacking multiple stretchable layers in smaller regions[8,25–36] to realize higher density functional electronics compared to single layer electronics[8,30]. In these works, how to interconnect electronic circuits and components is critically important consideration for design and fabrication. One strategy is based on intrinsically stretchable materials such as liquid metal[29,31,37,38] and conductive polymer[33–36]. They can intrinsically achieve high stretchability without complex patterning. Interconnection between layers is relatively easier through injection methods[31,39] although they require reliable sealing and packaging to avoid leakage, dehydration, disconnection from electronic components[8,40]. Another approach is structure-based multilayer stretchable devices with non-stretchable conductive metals deposited on stretchable structures[2,8,30]. The structure-based multilayer devices provide advantages of high conductivity, high scalability, and convenient interface with electronic components[41]. However, as more layers are integrated, overall degree of stretchability can be reduced because more regions are constrained by rigid components from each layer.

In this paper, we present our strategy to realize higher density stretchable electronics based on multilayer designs that affect minimally on mechanical strain although the number of layers increases. We provide the designs on forming interconnectors between rigid components on the multiple layers. The fabricated quadruple layer stretchable devices in a more compact form show similar degree of induced strain compared to a single layer device, as presented by the experimental results and computational analysis. We demonstrate the capability of the approach with the multilayer implantable bio-electronics and stretchable passive matrix LEDs.

Results

Vertically-separated multilayer stretchable circuit design

Three-dimensional structural circuit designs that maintain their stretchability over single-layer circuits provide advantages in packing electronics in smaller lateral space. Figure 1a shows a proposed 3D structural circuit design, named as a vertically-separated multilayer stretchable circuit (VSMSC) which consists of multiple layers of islands and stretchable interconnectors as illustrated in Fig. 1b. The island regions (non-stretchable, red dashed box in Fig. 1a) have multiple layers bonded top and bottom with interlayers (Fig. 1b) to allow for reliable formation and integration of vertical interconnect access (VIA) interconnectors and electrical components. The stretchable interconnectors (black box in Fig. 1a) of the VSMSC, however, are vertically separated without bonding layers (interlayers) as shown in

[1]School of Mechanical Engineering, Gwangju Institute of Science and Technology (GIST), Buk-gu, Gwangju 61005, Republic of Korea. [2]Electronics and Telecommunications Research Institute (ETRI), Daejeon 34129, Republic of Korea. ✉e-mail: jong@gist.ac.kr
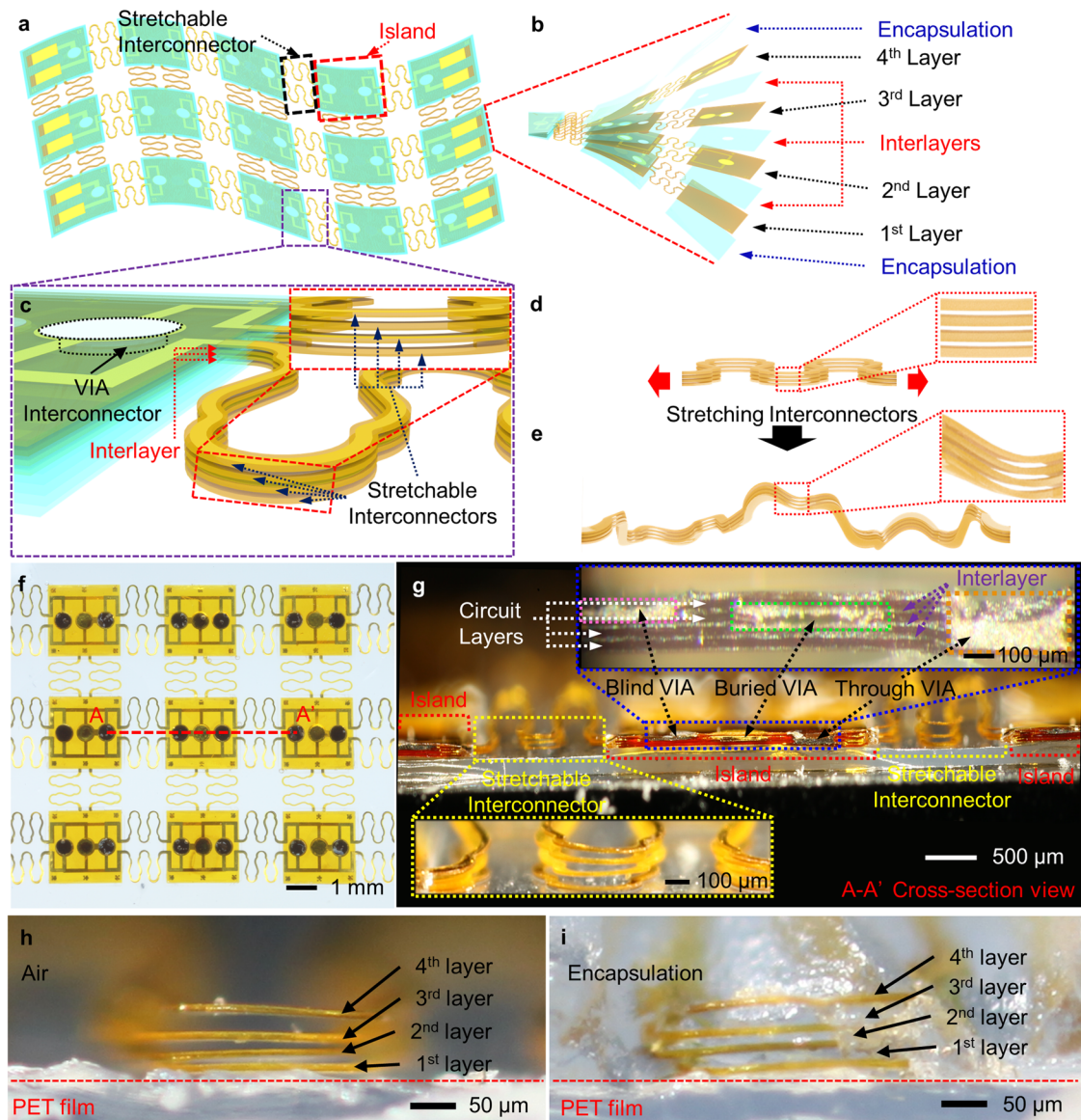
Fig. 1 | Vertically-separated multilayer stretchable circuit design. a Schematics of the Vertically-Separated Multilayer Stretchable Circuit (VSMSC). The islands (red box) are non-deformable regions designated for assembling rigid components. The vertically-separated stretchable interconnectors (black box) are deformable regions to absorb strain more efficiently. **b** Exploded schematics of the VSMSC with quadruple layers. The rigid interlayers (cyan, SU8) are only formed between the island layers, not between the stretchable interconnector layers. **c** 3D illustration of the assembled VSMSC. The stretchable interconnectors are vertically separated. The circuit layers are vertically interconnected through via holes in the island. **d, e** 3D illustration of the vertically separated stretchable interconnectors (**d**) before stretching and (**e**) after stretching. **f** Optical image of the fabricated VSMSC with quadruple layers. **g** Optical image of cross-sectional side view of the VSMSC. The stretchable multi-layer interconnectors are separated vertically. The separated interconnectors are electrically connected through three different types of VIAs (Dashed boxes: Blind (Magenta), Buried (Green), Through (Orange)) in non-deformable islands. **h, i** Micrographs of side views of the vertically separated stretchable interconnectors (**h**) before and (**i**) after low modulus silicone encapsulation.

Fig. 1c. The design provides advantages of deforming interconnectors (mainly absorbing strains) more freely and individually as in Fig. 1d, e when external forces such as loads to stretch are applied.

Figure 1f shows an optical image of a stretchable electronics with the VSMSC designs including quadruple layers of circuits. Each circuit layer was fabricated by depositing and photolithographically defining metal electrodes (Ti/Au = 30/200 nm) on a polyimide (PI) film (5 µm) and encapsulating by another PI layer (5 µm). The VIA holes interconnecting the circuit layers vertically were formed on the matching PI films, stacked with the aid of the interlayers (SU-8, thickness: 5 µm), and filled with conductive epoxy (H20E, EPO-TEK Inc., USA). More details of the interconnections and fabrication processes are in Supplementary information (Supplementary Fig. 1, 2) and the Methods.

The cross-sectional optical image in Fig. 1g shows the three types of via holes (blue dashed boxes: blind, buried, through) interconnectors the circuit layers vertically depending on circuit design. The optical image in the yellow dotted box also clearly shows that the stretchable interconnectors are vertically separated. The VSMSC is encapsulated with low modulus silicone (Ecoflex 00-30, Smooth-On, Inc., USA, Young's modulus: ~125 kPa) for maintaining separation of the stretchable interconnectors even under deformations and using conveniently. Figure 1h, i show optical images of the stretchable interconnectors before (Fig. 1h) and after (Fig. 1i) encapsulation. Separations between stretchable interconnectors of each layer keep their original position during the encapsulation process. More details of the encapsulation process are in the Methods.

Mechanical characteristics of the VSMSC

The VSMSC design providing a more compact form factor is efficient in absorbing strains in response to mechanical deformations such as bending or stretching. Figure 2a, b shows the fabricated quadruple layers VSMSC and corresponding finite element models (FEM) except low modulus silicone encapsulation under bending (radius: 3 mm) and stretching (30%

stretching for one island-stretchable interconnectors unit). The maximum tensile (positive) and compressive (negative) strains are observed at the stretchable interconnectors rather than the VIA interconnectors embedded in the islands as bending stiffness (EI, E: elastic modulus, I: the second moment of area) of the vertically separated interconnectors is much lower. More details are in Supplementary information (Supplementary Fig. 3).
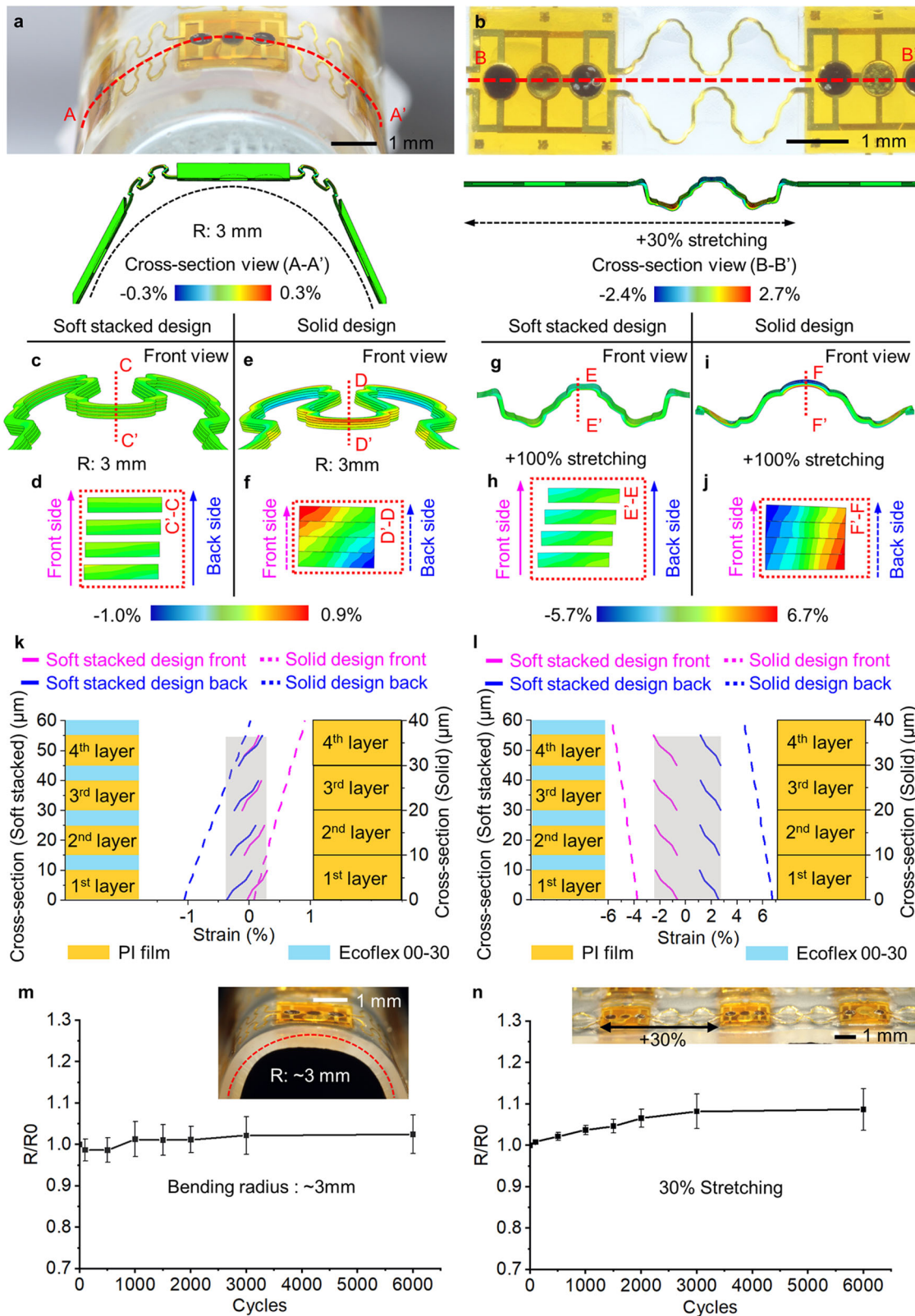
Fig. 2 | Mechanical characteristics of the VSMSC. a, b Optical images and corresponding finite element (FE) analysis models of the VSMSC except for low modulus silicone encapsulation (**a**) bent at a radius of 3 mm and (**b**) stretched at 30%. Most of strain noted by the color maps is absorbed in the interconnectors instead of the islands. **c–f** Comparison of (**c, d**) the soft stacked and (**e, f**) solid designs when bending at a radius of 3 mm. The maximum strain (0.29%) of the soft stacked design is much lower than that (0.9%) of the solid design. **g–j** Comparison of (**g–h**) the soft stacked and (**i, j**) solid designs when stretching 100% of the interconnectors. The maximum strain (2.7%) of the soft stacked design is much lower than that (6.74%) of the solid design. **k, l** Strain distributions through the cross-sectional dimension of the soft stacked design (solid lines) and solid design (dashed lines) when (**k**) bending and (**l**) stretching. The strain at the front side (magenta) and the back side (blue) of the soft stacked design is confined between −0.37% and 0.29% for bending and between −2.42.% and 2.7% for stretching while the solid design has much higher strain (between 1.06% and 0.9% for bending, between −5.72% and 6.74% for stretching). **m, n** Measurement results of relative resistance of the fabricated VSMSC (**m**) for repetitive bending (bending radius: 3 mm) and (**n**) repetitive stretching (stretchability: 30%) up to 6000 cycles. ($n = 6$ samples each for bending and stretching, data presented as mean ± s.d.).

Figure 2c–j show a comparison of FEM results for quadruple layer stretchable interconnectors of the low modulus silicone encapsulated VSMSC (Fig. 2c, d, g, h, soft stacked design) and solid multilayer circuit (Fig. 2e, f, i, j, solid design) when bending (r: 3 mm) and stretching (100%). The FEM results indicate only stretchable interconnectors except for silicone encapsulation to distinguish strain differences. When bending (Fig. 2c–f), the quadruple layers in the soft stacked design slide gradually, absorb strains, resulting in very low strain (tensile: 0.3%, compressive: 0.3%) in the interconnectors (Fig. 2d). On the other hand, in the solid design, strains are much more concentrated (about 3 times, tensile: 0.9%, compressive: 1.0%) in the interconnectors (Fig. 2f). When stretching (Fig. 2g–j), similarly, the VSMSC interconnectors induce very low strain (tensile: 2.7%, compressive: 2.4%, Fig. 2h) while the solid design does more than double strain (tensile: 6.7%, compressive: 5.7%, Fig. 2j).

More direct comparisons between the soft stacked and solid designs are plotted in Fig. 2k (for bending) and 2 l (for stretching). We plotted and compared surface strains because strains are usually maximum on surfaces and they can cause premature failure on the interconnectors[42]. When bending on a radius of 3 mm, the tensile and compressive deformation occurs on the front and back surfaces of the interconnectors as in Fig. 2c–f. However, the tensile (magenta solid line) and compressive (blue solid line) strains of the soft stacked design stay within the narrower bounds (−0.3–0.3%, gray region) compare to the solid design (magenta and blue dashed lines, −1.0–0.9%) as in Fig. 2k because the soft stacked design connected with the low modulus silicone isolates strain propagation to other layers[42,43]. More details about strain distribution depending on interlayer thickness are in Supplementary information (Supplementary Fig. 4). The results are similar when stretching the interconnectors, the soft stacked design builds less strain (−2.4–2.7%, solid lines) than the strain (−5.7–6.7%, dashed lines) as plotted in Fig. 2l because the soft stacked design exhibits almost same degree strains of a single layer interconnector as in Supplementary information (Supplementary Fig. 5).

The fabricated quadruple VSMSC is durable enough to maintain its mechanical and electrical stability when subjected to cyclic deformations of bending (radius: 3 mm, Fig. 2m) and stretching (+30%, Fig. 2n) using the motorized microstage. In both types of deformation, the electrical resistance was maintained without significant change or breaking. Mechanical degradation was not observed in the multilayer structure after repetitive deformation over 6,000 cycles.

Implantable bio-electronics design based on the VSMSC

As the multilayer design reduces lateral size while maintaining robustness to deformation, it is useful in applications like implantable bio-electronics which require a small but stretchable form factor. Figure 3a illustrates one of the bio-electronics working as a pacemaker that reads an electrocardiogram (ECG) signals from the heart, filtering noise through a low pass filter, processing, and decision-making in a microprocessor unit (MCU) to generate artificial pulses through electrodes as shown with the diagram in Fig. 3b. The bio-electronics was designed in a 3 × 3 islands-based quadruple VSMSC with low modulus silicone encapsulation to be implantable under the dermis as in Fig. 3c. The layer-by-layer design is shown in Fig. 3d. The bio-electronics includes 22 electronic components integrated on the top layer (4th layer), sensing and stimulating electrical pads facing down on the bottom layer (1st layer), and three-dimensional interconnectors in the middle layers (2nd, 3rd layer). More details of the design is in Supplementary information (Supplementary Fig. 7).

The fabricated bio-electronics with the quadruple layer VSMSC in Fig. 3e is a quarter smaller than the single layer design. (Fig. 3f) But deformable enough to be squeezed as shown in Fig. 3g. These characteristics allow the implanted bio-electronics to be deformed without causing too much stress to surrounding live tissues as in Fig. 3h. In vivo experiments indicate that squeezing from outside did not cause any damage to the implanted quadruple VSMSC bio-electronics as demonstrated by reading ECG signals (black) and stimulating the heart (blue, starting at 4.5 s) in Fig. 3i. It should be noted that electrical powering and data acquisition for ECG and stimulation signals were conducted through external wires because the implant was not equipped with standalone circuits, memories and batteries yet as we focused more on stretchable designs and characteristics. In addition, the stimulation signals were generated from the same type of the external MCU because thresholds to count pulses should be adjustable for each mouse model. The measured ECG signal (black) from our bio-electronics is comparable with the measurement (red) from a commercial ECG sensor (EVAL-AD8233, Analog Devices, USA). More details of the in vivo experimental process are in the Methods and Supplementary information (Supplementary Fig. 8).

We evaluated the durability of the VSMSC-based bio-electronics by implanting and keeping it in a live mouse model for two weeks. After 2 weeks, the incision was healed clearly and the bio-electronics was settled stably under the skin as shown in Fig. 3j. The bio-electronics withdrawn from the mouse model was mechanically stable (no mechanical damage found). The bio-electronics was still capable of sensing the ECG signals (Fig. 3k) and generating stimulating signals (Fig. 3l) when evaluated on a human chest with external wirings for powering and data acquisition despite repetitive random deformations caused by the free movement of the mouse for two weeks. It should be noted that biocompatibility and cytotoxicity of bio-electronics is critically important consideration. The devices are fully encapsulated with soft elastomer which is known to be biocompatible[44] and the solid components do not usually leach cytotoxic elements through elastomeric encapsulants[45]. Although the incision was healed clearly and the device was settled stably under the skin after two weeks of implantation, more systematic assessments are required for long-term biocompatibility for practical applications. More details of the experimental process and measurements are in the Methods and Supplementary information (Supplementary Fig. 9, 10).

Passive matrix LED display based on the VSMSC design

The VSMSC design is convenient in interconnecting repetitive electronic devices to be controlled individually. As a demonstrator, we fabricated a passive matrix light-emitting diodes (LEDs) array whose individual devices can be turned on and off by externally powering the target devices as sketched in Fig. 4a. The double-layer VSMSC provides traces (Magenta) for the anodes (+) and traces (Blue) for the cathodes (−) as in Fig. 4b. The top and bottom traces do not electrically cross each other as the cathodes are interconnected to the bottom layer through via holes. (cross-sectional view in Fig. 4b).

Figure 4c shows the 6 × 6 double-layer VSMSC passive matrix LEDs array. The individual LEDs can be independently controlled as displayed in the alphabet letters ('G', 'I', 'S', and 'T') in Fig. 4d–g. The double-layer
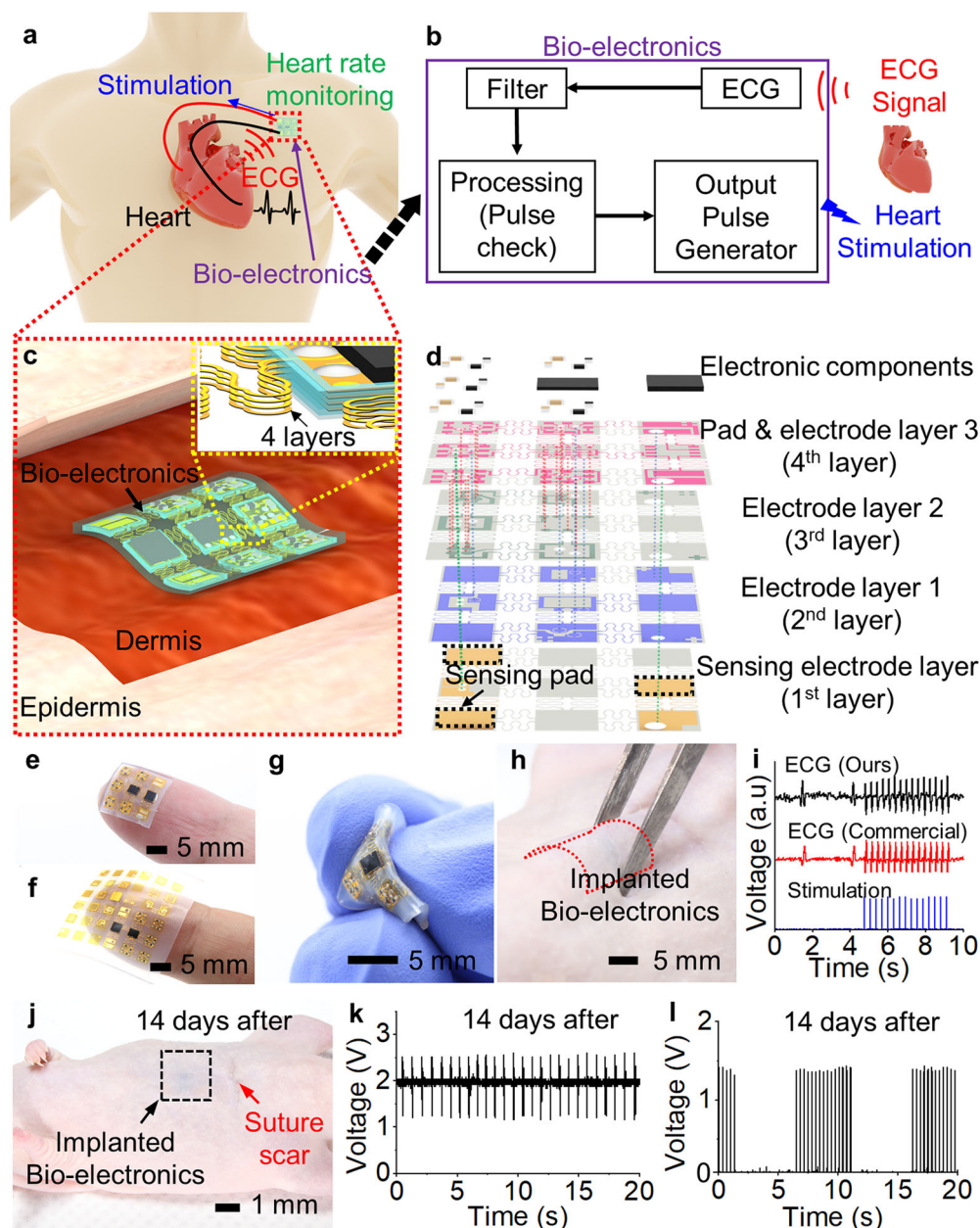
Fig. 3 | Implantable bio-electronics design based on the VSMSC. a Fundamental functions of the implantable bio-electronics include electrocardiogram (ECG) measurement, heart rate monitoring, and stimulation. **b** Process flow diagram of the bio-electronics. **c** Illustration of the subcutaneous bio-electronics based on the VSMSC design with quadruple layers. **d** Circuit layer design of the bio-electronics. **e**, **f** Photographs of the fabricated bio-electronics (**e**) with the quadruple layer VSMSC and (**f**) with the single layer circuit placed on a finger. **g** Photographs of the fabricated bio-electronics squeezed by fingers. **h** Optical image of pinching the implanted bio-electronics after being cured for 2 weeks. **i** ECG signals measured from the fabricated bioelectronics (Ours, black) with implantation and commercial (red) device with attaching to the skin. The blue signal is a stimulating signal started automatically around 4.5 s after detecting the bradycardia state of the heart. **j** Photograph of a mouse model with the implanted bio-electronics during 14 days for in vivo experiment. **k, l** (**k**) ECG and (**l**) stimulation signals of the bio-electronics for estimating functional performance after 14 days in vivo experiment.

VSMSC LED passive matrix is stretchable enough to absorb strain for various deformations such as bending (Fig. 4h, bending radius: 3 mm), stretching (Fig. 4i, 50% stretch of one island-stretchable interconnectors unit), and twisting (Fig. 4j, twisting angle 180°). Repetitive bending cycles at a radius of 4 mm did not show any electrical degradation (Fig. 4k). Figure 4l shows the current-voltage (I-V) curves of the LED matrix after stretching at degrees of stretchability (10–50%, Fig. 4i). The IV curves are almost identical. Repetitive stretching cycles (30% uniaxial) did not show a significant difference in the forward voltage (ΔV_F at 40 mA) of the double-layer VSMSC LED matrix as shown in Fig. 4j. It should be noted that a fill factor of LED arrays is crucial for high-resolution displays. Although the fill factor of the passive matrix LED array is relatively low (~36%, rigid parts) as they were fabricated in the individual university lab, we expect that modular design[46], an imbricate scale design[47], and a morphable design[48], would improve a fill factor significantly for high resolution displays.

Discussion

Although we demonstrated mechanical durability of the vertically-separated multilayer stretchable circuit by repetitive bending and stretching, the devices would require additional strain-limiting designs for daily uses to avoid mechanical failure when stretched excessively, beyond the designed stretchability. We expect that the devices would be minimally
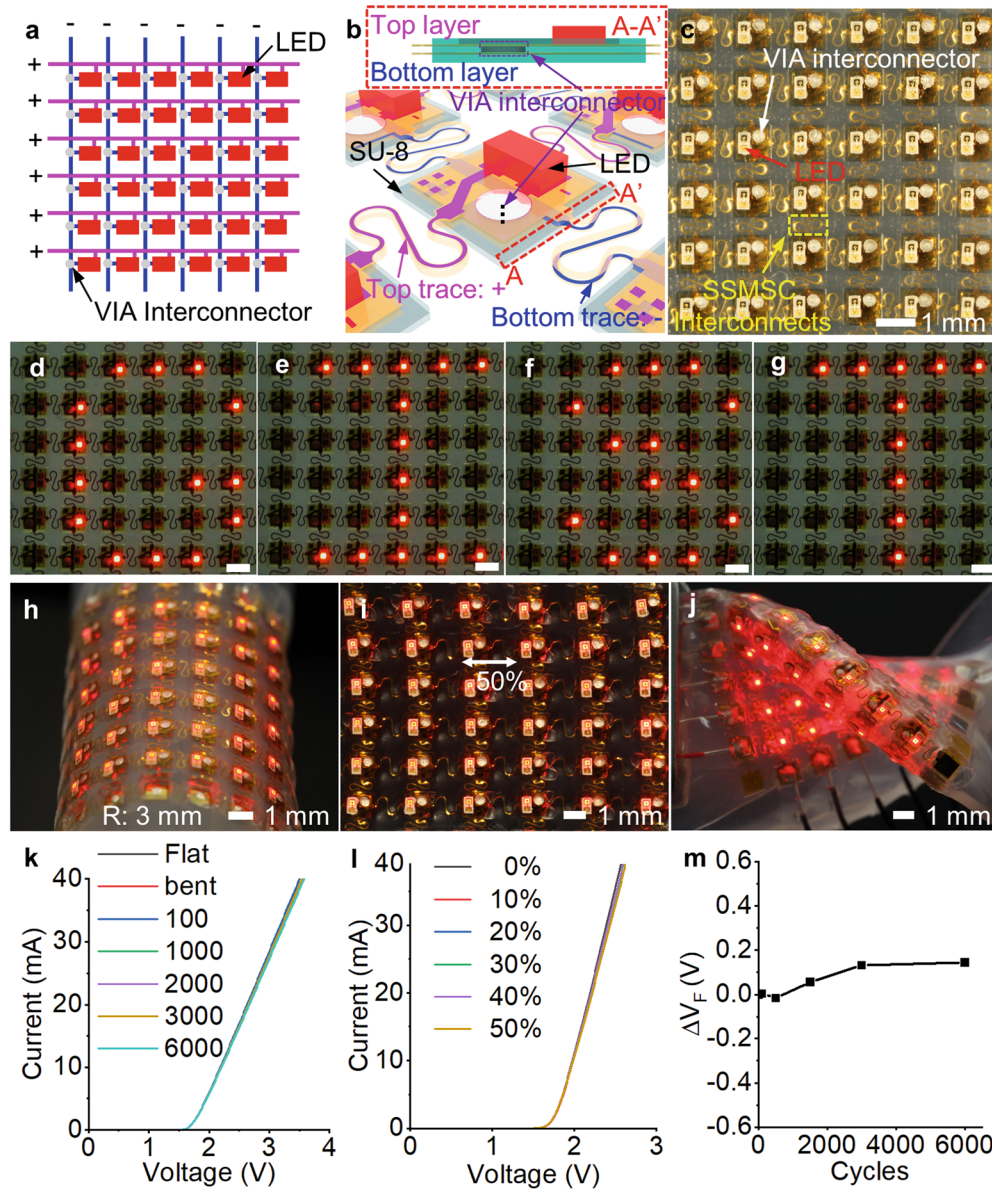
Fig. 4 | Passive matrix LED display based on the VSMSC design. a Schematic diagram of the LED passive matrix with the VSMSC double layers design. **b** Elevated view of the design. The positive ('+', magenta) and negative ('−', blue) electrodes of the LEDs are interconnected through the top and bottom layer of the stretchable interconnectors, respectively. **c** Optical image of the fabricated LED passive matrix with the VSMSC design (6 × 6). **d–g** Alphabet letters 'G', 'I', 'S', and 'T' displayed with the double-layered LED passive matrix. Scale bar: 1 mm. **h–j** Mechanical deformations of the double-layered LED passive matrix with LEDs on while (**h**) bending (bending radius: 3 mm), (**i**) stretching (one island-stretchable interconnectors unit stretchability: 50%), and (**j**) twisting (twisting angle: ~180°). **k** Current-voltage (I-V) curves of the LED passive matrix after repetitive bending cycles (bending radius: 4 mm). **l** I-V curves with different degrees of stretchability. **m**. Forward voltage difference (ΔV_F) at 40 mA of the double-layered LED passive matrix under repetitive stretching (30%) up to 6000 cycles.

affected by environmental temperature (less than 100 °C or so) as the devices are fabricated with the materials and components durable at the daily temperature range. Although we used inorganic electrical components and metal interconnects fully encapsulated with elastomeric layers, excessive exposure to humidity for a long time may cause failure and lower performance, e.g., higher resistance. In the cases, the devices may require additional encapsulating layers, e.g., Parylene, to improve moisture resistance[49,50].

In summary, the results presented here indicate that the multilayer designs with the multilayer stretchable interconnectors and rigid islands can provide a degree of stretchability, comparable to a single layer design, while maintaining in compact size, e.g., four times smaller than a single layer design. The feature is enabled by the vertically-separated multilayer stretchable design which induces multiple interconnectors to deform individually, reducing mechanical strain smaller than solid stacked multilayer structure. We demonstrated the benefits of the design with a compact stretchable implant and passive matrix LEDs array. The in vivo experiments with the implant connected with external wires for powering and data acquisition demonstrated that the design is effective in reducing lateral size of bio-electronic implants. The multilayer stretchable LED passive matrix also demonstrated that the design is useful for circuits requiring crossing traces. This approach will possibly lead to efficient design methods for stretchable electronics with complex circuits, however, independent interconnectors and whole device-covered elastomeric encapsulation make limitations for reducing device size and stretchability. The design and fabrication strategies should be useful for more complex and multifunctional stretchable devices that require more compact size.

Methods

Preparation of the stretchable electronic circuit layers

The stretchable electronic circuit layer consisting of islands and serpentine interconnectors was formed on a PI film (Polyimide, ~5 μm) which was temporarily attached to a silicone layer (10:1 Polydimethylsiloxane (PDMS), ~3 μm, Sylgard184, Dow corning, USA) coated on a glass slide (Micro glass substrate, Matsunami Glass) as a temporary carrier. Sputtering followed by wet chemical etching formed metal traces (Ti/Au: 30 nm / 200 nm) on the PI film. Another PI layer (~5 μm) through spin-casting and curing PI solution encapsulated the metal traces. Reactive ion etching with oxygen plasma over a titanium mask (mask thickness: ~30 nm) formed the stretchable electronic circuit layers and exposed electrode pads.

Preparation of the vertically-separated multilayer stretchable circuit (VSMSC)

The VSMSC was formed by alternatively stacking an epoxy layer (SU-8 2000 series negative photoresist, Kayaku advanced materials Inc., USA) and the stretchable electronic circuit layer as shown with the schematic image of the structure in Fig. 1b. We chose SU-8 to form the interlayers because SU-8 could be conveniently used to form micro-structures through photolithography and low temperature baking (85 °C)[51,52]. As a carrier substrate, we used a polyethylene terephthalate (PET) film attached on a PDMS glass slide. After forming a base epoxy layer (SU-8, thickness: ~3 μm) on the carrier substrate, we formed another epoxy layer on the backside of the first stretchable electronic circuit layer picked by a thermal release tape (Graphene square Inc. South Korea). After aligning and bonding the stretchable electronic circuit layer on the PET film by heating and pressing (85 °C, 70 kPa) for 10 min, we removed the thermal release tape by heating on a hot plate (110 °C, 10 min). We repeated stacking the epoxy layers and the stretchable electronic circuit layers for the VSMSC. The silver conductive epoxy is initially fluidic and thermally curable, so we could electrically interconnect the multilayers by filling the VIA (vertical Interconnect Access) holes, followed by thermal curing (110 °C, 2 h). The vertical interconnect access (VIA) interconnectors to electrically connect between desired layers were formed with silver conductive epoxy (H20E, EPO-TEK Inc., USA) through the holes made by the reactive ion etching process. While the blind and through VIAs could be formed after stacking all the circuit layers, the buried VIA was formed after stacking the corresponding middle circuit layers. For reliable use, the VSMSC was encapsulated with low modulus silicone (Ecoflex 00-30, Smooth-On, Inc., USA) by filling the VSMSC with a prepolymer slowly from bottom to top to prevent the separate interconnectors from merging each other. The bottom of the VSMSC was also encapsulated after removing the VSMSC from the carrier substrate. More details are in Supplementary information (Supplementary Fig. 2).

Finite element method (FEM) simulation

The characteristics for mechanical bending and stretching deformation were analyzed using the FEM (ABAQUS). The geometry models employ an 8-node, linear hexahedral solid element C3D8R. The solid parts were physically bonded together as the nodes were shared for their adhered elements. Deformations such as bending or stretching were implemented by linear displacement at the boundaries. We used the following material properties and dimensions for the simulations, each layer material (polyimide (PI)): Young's modulus $E_{pi} = 2.5$ GPa, Poisson's ratio $= 0.34$, thickness $t_{pi} = 10$ μm, inter layer material (SU-8): Young's modulus $E_{SU-8} = 4.02$ GPa, Poisson's ratio $= 0.22$, thickness $t_{SU-8} = 5$ μm, metal trace(Au): Young's modulus $E_{Au} = 74$ GPa, Poisson's ratio $= 0.42$, thickness $t_{Au} = 200$ nm, encapsulation (Ecoflex 00-30): Young's modulus $E_{ecoflex} = 125$ kPa, Poisson's ratio $= 0.49$, thickness $t_{ecoflex} = 5$ μm.

Preparation of the implantable bio-electronics

The implantable bio-electronics was designed based on the 4-layers VSMSC. Each layer includes encapsulated metal traces in a structure of PI-Ti/Au-PI (thickness: 5 μm - 30 nm/200 nm - 5 μm). Some parts of the metal trace layers were exposed at the places where VIA interconnectors, electronic components, and tissue interfaces were required. The bottom circuit layer was fabricated to face down for direct contact with live tissues. The electronic components integrated on the islands of the top layer using conductive adhesive (H20E, EPO-TEK, USA) were mechanically reinforced with an optical adhesive (NOA61, Norland Products, USA). The fabricated bio-electronics were fully encapsulated with the low modulus silicone (Ecoflex 00-30) except the electrode area for direct contact with live tissues. More details are in Supplementary information (Supplementary Fig. 2).

Preparation of the passive matrix stretchable LED display

The passive matrix stretchable LED display was designed to have the 2-layers VSMSC and 7×7 islands. The one row and column of islands were assigned to have electrical pads for external wiring for powering and driving the display. The other 6×6 islands serve as pixels with one inorganic red LED (APG0603sec-e-tt, Kingbright, USA) and one VIA interconnector on each island. The 2-layers design with the VSMSC and VIA interconnectors enables independent external electrical connection (positive and negative electrodes) for each LED for the 6 × 6 stretchable inorganic LED matrix. For the controlled display operations, we connected the prepared passive matrix LED display with a microprocessor unit (Arduino Mega, Arduino, USA) and a display driver (MAX7219, Analog Devices, USA). More details of the various deformations including repetitive bending and stretching during the scrolling display operation of stretchable LED display are in Supplementary Video 1.

Measurements of electrical properties

The resistances of the VSMSCs were measured with a digital multimeter unit (34461 A, Keysight technologies, USA). For reliable measurements, we fixed the external wires strongly on the stage to minimize external disturbances other than changes caused by deformations such as bending or stretching. The current-voltage characteristics and the forward voltages of the LED matrix were measured with a source measure unit (B2902A, Keysight technologies, USA) with the pulsed sweep mode (pulse period: 110 ms, pulse width: 10 ms) to reduce residual temperature caused by previous measurements.

Repetitive deformation experiments

The repetitive bending and stretching deformations of the VSMSC and the passive matrix LED display were conducted on a custom-built motorized microstage consisting of the motor driver, the LabVIEW based controller, and the sample mounter. The stage can be controlled to move at a resolution of 0.1 μm. One end of the sample (VSMSC or LED display) was fixed on a ground stage and the other end of the sample were leveled and fixed on the movable microstage which can be controlled to move repetitively along one direction. The custom microstage was programmed to measure and record the resistances of the VSMSC and the current-voltage curves of the passive matrix LED display in between repetitive deformation cycles. More details are in Supplementary information (Supplementary Fig. 6).

Animal experiments

In vivo experiments of the implantable bio-electronics were conducted with hairless mice (SKH1-Hr^hr, 12–16 weeks old, ~30 g). The mice were put under general anesthesia by intraperitoneal injection of a mixture of ketamine (50 mg Kg^{-1}, Yuhan Ketamine 50, Yuhan corp., Republic of Korea), xylazine (5 mg Kg^{-1}, Rompun Inj., Bayer corp., Germany), and saline solution (Normal Saline Inj., Dae Han Pharm Co. Ltd., Republic of Korea). The bio-electronics was inserted under ventral skin of the mice through small incision (~15 mm) which was later sutured 4-5 stitches. Electrical wires were connected externally for powering, measuring the ECG, and stimulating the heart. A commercially available ECG sensor (EVAL-AD8233, Analog Devices, USA) was set

up for comparison with the ECG from the implanted bio-electronics. After setting up the bio-electronics, we measured the ECG signals from both devices as a normal state (~102 beats per minute (bpm)). To estimate the pacemaker performance of the bio-electronics, we conducted a thoracotomy to expose the heart that causes the diaphragm to rupture, as a result, the bradycardia state (< 66 bpm) is induced[13]. The implanted bio-electronics is checking the heart rate, when the bradycardia state is measured, the MCU generates stimulation signals (180 bpm) through two external wires connected with the bio-electronics. The stimulation signals from the bio-electronics were directly applied to the heart after a thoracotomy. The ECG and stimulation signals were monitored and recorded with an oscilloscope (DSO-X 2024 A, Agilent Technologies, Inc., USA). The in vivo durability test was conducted after implantation of the bio-electronics and suturing process under general anesthesia. The ECG and stimulation signals were measured through external wire electrodes on a human chest for electrical powering and data acquisition before and after withdrawal from the animal model 2 weeks after implantation. More details of animal experiments are in Supplementary information (Supplementary Fig. 8, 9, 10). The animal experiments were conducted with approval from GIST Institutional Animal Care USE Committee (GIST-2020-052). The human subject experiments for verifying performances of the bio-electronics were conducted with informed consent obtained from all participants and granted exemption approval from the Institutional Review Board (IRB) of the GIST (20231225-HR-EX-011).

Data availability

Additional data related to this study may be requested from the corresponding author upon reasonable request.

References

1. Song, Y. M. et al. Digital cameras with designs inspired by the arthropod eye. *Nature* **497**, 95–99 (2013).
2. Sim, K. et al. Three-dimensional curvy electronics created using conformal additive stamp printing. *Nat. Electron.* **2**, 471–479 (2019).
3. Kim, K. et al. All-printed stretchable corneal sensor on soft contact lenses for noninvasive and painless ocular electrodiagnosis. *Nat. Commun.* **12**, 1–11 (2021).
4. Kim, J. et al. Epidermal electronics with advanced capabilities in near-field communication. *Small* **11**, 906–912 (2015).
5. Kim, N., Lim, T., Song, K., Yang, S. & Lee, J. Stretchable multichannel electromyography sensor array covering large area for controlling home electronics with distinguishable signals from multiple muscles. *ACS Appl. Mater. Interfaces* **8**, 21070–21076 (2016).
6. Xu, B. et al. An epidermal stimulation and sensing platform for sensorimotor prosthetic control, management of lower back exertion, and electrical muscle activation. *Adv. Mater.* **28**, 4462–4471 (2016).
7. Hua, Q. et al. Skin-inspired highly stretchable and conformable matrix networks for multifunctional sensing. *Nat. Commun.* **9**, 1–11 (2018).
8. Song, H. et al. Highly-integrated, miniaturized, stretchable electronic systems based on stacked multilayer network materials. *Sci. Adv.* **3785**, 1–13 (2022).
9. Park, S. I. et al. Soft, stretchable, fully implantable miniaturized optoelectronic systems for wireless optogenetics. *Nat. Biotechnol.* **33**, 1280–1286 (2015).
10. Liu, Y. et al. Soft and elastic hydrogel-based microelectronics for localized low-voltage neuromodulation. *Nat. Biomed. Eng.* **3**, 58–68 (2019).
11. Herbert, R., Mishra, S., Lim, H. R., Yoo, H. & Yeo, W. H. Fully printed, wireless, stretchable implantable biosystem toward batteryless, real-time monitoring of cerebral aneurysm hemodynamics. *Adv. Sci.* **6**, 1901034 (2019).
12. Choi, Y. S. et al. Stretchable, dynamic covalent polymers for soft, long-lived bioresorbable electronic stimulators designed to facilitate neuromuscular regeneration. *Nat. Commun.* **11**, 1–14 (2020).
13. Jung, D. et al. Sustainably powered, multifunctional flexible feedback implant by the bifacial design and si photovoltaics. *Adv. Healthc. Mater.* **10**, 1–8 (2021).
14. Shin, J. H. et al. Wearable EEG electronics for a Brain–AI Closed-Loop System to enhance autonomous machine decision-making. *npj Flex. Electron.* **6**, 32 (2022).
15. Lee, Y. et al. Standalone real-time health monitoring patch based on a stretchable organic optoelectronic system. *Sci. Adv.* **7**, 1–11 (2021).
16. Lee, H. et al. Stretchable organic optoelectronic devices: design of materials, structures, and applications. *Mater. Sci. Eng. R. Rep.* **146**, 100631 (2021).
17. Ji, X. et al. An autonomous untethered fast soft robotic insect driven by low-voltage dielectric elastomer actuators. *Sci. Robot.* **4**, eaaz6451 (2019).
18. Byun, J. et al. Electronic skins for soft, compact, reversible assembly of wirelessly activated fully soft robots. *Sci. Robot.* **3**, 1–12 (2018).
19. Han, M. et al. Three-dimensional piezoelectric polymer microsystems for vibrational energy harvesting, robotic interfaces and biomedical implants. *Nat. Electron.* **2**, 26–35 (2019).
20. Qazi, R. et al. Wireless optofluidic brain probes for chronic neuropharmacology and photostimulation. *Nat. Biomed. Eng.* **3**, 655–669 (2019).
21. Fallegger, F., Schiavone, G. & Lacour, S. P. Conformable Hybrid Systems for Implantable Bioelectronic Interfaces. *Adv. Mater.* **32**, 1903904 (2020).
22. Song, Y., Min, J. & Gao, W. Wearable and implantable electronics: moving toward precision therapy. *ACS Nano* **13**, 12280–12286 (2019).
23. Hong, S. Y. et al. High-density, stretchable, all-solid-state microsupercapacitor arrays. *ACS Nano* **8**, 8844–8855 (2014).
24. Oh, H. et al. High density integration of stretchable inorganic thin film transistors with excellent performance and reliability. *Nat. Commun.* **13**, 1–9 (2022).
25. Kim, D. H. et al. Stretchable and foldable silicon integrated circuits. *Nature* **320**, 507–511 (2008).
26. Guo, L. & DeWeerth, S. P. High-density stretchable electronics: toward an integrated multilayer composite. *Adv. Mater.* **22**, 4030–4033 (2010).
27. Xu, R. et al. Designing thin, ultrastretchable electronics with stacked circuits and elastomeric encapsulation materials. *Adv. Funct. Mater.* **27**, 1–12 (2017).
28. Tang, L., Shang, J. & Jiang, X. Multilayered electronic transfer tattoo that can enable the crease amplification effect. *Sci. Adv.* **7**, eabe3778 (2021).
29. Liu, S., Shah, D. S. & Kramer-Bottiglio, R. Highly stretchable multilayer electronic circuits using biphasic gallium-indium. *Nat. Mater.* **20**, 851–858 (2021).
30. Huang, Z. et al. Three-dimensional integrated stretchable electronics. *Nat. Electron.* **1**, 473–480 (2018).
31. Green Marques, D., Alhais Lopes, P., De Almeida, A. T., Majidi, C. & Tavakoli, M. Reliable interfaces for EGaln multi-layer stretchable circuits and microelectronics. *Lab Chip* **19**, 897–906 (2019).
32. Li, G. et al. High-efficiency large-area printed multilayer liquid metal wires for stretchable biomedical sensors with recyclability. *ACS Appl. Mater. Interfaces* **13**, 56961–56971 (2021).
33. Liu, X. et al. Biomimetic integration of tough polymer elastomer with conductive hydrogel for highly stretchable, flexible electronic. *Nano Energy* **92**, 106735 (2022).
34. Stier, S. P. & Böse, H. Electroplating and ablative laser structuring of elastomer composites for stretchable multi-layer and multi-material electronic and sensor systems. *Micromachines* **12**, 1–17 (2021).

35. Lopes, P. A. et al. Bi-Phasic Ag-In-Ga-embedded elastomer inks for digitally printed, ultra-stretchable, multi-layer electronics. *ACS Appl. Mater. Interfaces* **13**, 14552–14561 (2021).
36. La, T. G. et al. Two-layered and stretchable e-textile patches for wearable healthcare electronics. *Adv. Healthc. Mater.* **7**, 1801033 (2018).
37. Kim, M. S. et al. Stretchable printed circuit board based on leak-free liquid metal interconnection and local strain control. *ACS Appl. Mater. Interfaces* **14**, 1826–1837 (2022).
38. Jung, W. et al. Solvent-assisted filling of liquid metal and its selective dewetting for the multilayered 3D interconnect in stretchable electronics. *ACS Nano* **16**, 21471–21481 (2022).
39. Fassler, A. & Majidi, C. 3D structures of liquid-phase GaIn alloy embedded in PDMS with freeze casting. *Lab Chip* **13**, 4442–4450 (2013).
40. Tee, B. C. K. & Ouyang, J. Soft Electronically Functional Polymeric Composite Materials for a Flexible and Stretchable Digital Future. *Adv. Mater.* **30**, 1802560 (2018).
41. Xue, Z., Song, H., Rogers, J. A., Zhang, Y. & Huang, Y. Mechanically-guided structural designs in stretchable inorganic electronics. *Adv. Mater.* **32**, 1–32 (2020).
42. Su, Y., Li, S., Li, R. & Dagdeviren, C. Splitting of neutral mechanical plane of conformal, multilayer piezoelectric mechanical energy harvester. *Appl. Phys. Lett.* **107**, 041905 (2015).
43. Shi, Y., Rogers, J. A., Gao, C. & Huang, Y. Multiple neutral axes in bending of a multiple-layer beam with extremely different elastic properties. *J. Appl. Mech. Trans. ASME* **81**, 1–4 (2014).
44. Bae, W. J. et al. AB168. Evaluation of the biocompatibility of packing materials for a catheter. *Transl. Androl. Urol.* **4**, AB168 (2015).
45. Song, K. et al. Subdermal flexible solar cell arrays for powering medical electronic implants. *Adv. Healthc. Mater.* **5**, 1572–1580 (2016).
46. Kim, N., Kim, J., Seo, J., Hong, C. & Lee, J. Stretchable inorganic LED displays with double-layer modular design for high fill factor. *ACS Appl. Mater. Interfaces* **14**, 4344–4351 (2022).
47. Su, Y. et al. Mechanics of stretchable electronics with high fill factors. *Int. J. Solids Struct.* **49**, 3416–3421 (2012).
48. Lee, Y., Kim, B. J., Hu, L., Hong, J. & Ahn, J. H. Morphable 3D structure for stretchable display. *Mater. Today* **53**, 51–57 (2022).
49. Menon, P. R., Li, W., Tooker, A. & Tai, Y. C. Characterization of water vapor permeation through thin film parylene C. *TRANSDUCERS 2009-2009 Int. Solid-State Sensors, Actuators Microsystems Conf. IEEE* 1892–1895 (2009).
50. Ortigoza-Diaz, J. et al. Techniques and considerations in the microfabrication of parylene c microelectromechanical systems. *Micromachines* **9**, 422 (2018).
51. Agirregabiria, M. et al. Fabrication of SU-8 multilayer microstructures based on successive CMOS compatible adhesive bonding and releasing steps. *Lab Chip* **5**, 545–552 (2005).
52. Steigert, J. et al. A versatile and flexible low-temperature full-wafer bonding process of monolithic 3D microfluidic structures in SU-8. *J. Micromech. Microeng.* **18**, 095013 (2008).

Author contributions
J.L. planned and supervised the concept. D.J. fabricated the device, performed electrical and mechanical measurements. H.J. T.L. contributed mechanical characterization and gave advice and discussion on the concept. S.C gave advice and discussion on the vertically bonding process. D.J., C.H. performed the animal surgeries. J.L. and D.J. wrote the manuscript. All authors read and commented on the manuscript.

Competing interests
The authors declare no competing interests.

Additional information
Supplementary information The online version contains Supplementary Material available at https://doi.org/10.1038/s41528-024-00299-y.

Correspondence and requests for materials should be addressed to Jongho Lee.

Reprints and permissions information is available at http://www.nature.com/reprints

Publisher's note Springer Nature remains neutral with regard to jurisdictional claims in published maps and institutional affiliations.